Classical Bifurcation and Enhancement of Quantum Shells

— Systematic Analysis of Reflection-Asymmetric Deformed Oscillator —

Ken-ichiro ARITA* and Kenichi MATSUYANAGI
Department of Physics, Kyoto University, Kyoto 606-01, Japan
(April, 1995)

Correspondence between classical periodic orbits and quantum shell structure is investigated for a reflection-asymmetric deformed oscillator model as a function of quadrupole and octupole deformation parameters. Periodic orbit theory reveals several aspects of quantum level structure for this non-integrable system. Good classical-quantum correspondence is obtained in the Fourier transform of the quantum level density, and importance of periodic orbit bifurcation is demonstrated. Systematic survey of the local minima of shell energies in the two-dimensional deformation parameter space shows that prominent shell structures do emerge at finite values of the octupole parameter. Correspondences between the regions exhibiting strong shell effects and the classical bifurcation lines are investigated, and significance of these bifurcations is indicated.

Contents

---

*Present address: *Yukawa Institute for Theoretical Physics, Kyoto University, Kyoto 606-01, Japan.*

1. INTRODUCTION

Shell structure is one of the important aspects of finite quantum many-body systems. In the single-particle level density, one may generally find some regular patterns like shells consisting of dense and thin regions. This pattern changes with deformation, and the system favors the shape which makes the level density at the Fermi surface lower. Predictions of the superdeformed (extremely large quadrupole deformations with axis ratio about 2:1) and the hyperdeformed (the axis ratio about 3:1) nuclear states, which are hot current topics of high-spin nuclear structure physics, had been based on the above kind of consideration. Strong shell effects which appear at ellipsoidal shapes with the axis ratios about 2:1 and 3:1 play essential roles in stabilizing such exotic shapes. Reflection-asymmetric degrees of freedom are also one of the most exciting subjects in the current high-spin physics. Superdeformed potentials possess remarkable single-particle level structures where levels with different parities approximately (exactly in the harmonic oscillator limit) degenerate in the same major shell, which may bring about strong octupole correlations [1–3]. Recent remarkable development of large γ-ray detector arrays encourages us to find such exotic shapes like reflection-asymmetric superdeformations, and to investigate the mechanism of producing them. Recently micro-cluster physics have also attracted much attentions, and many nuclear physicists have been contributing to this new field. Shell structures and deformations of clusters are very interesting subjects — their shapes can actually be seen with an electron microscope — , and one can apply almost the same theoretical framework to both nuclei and micro-clusters [4–6].

A clear understanding of the origin of shell structure may be obtained by the use of semiclassical theory. Correspondences between quantum spectra and classical dynamical properties of Hamiltonian systems have been extensively investigated for two limiting cases, namely, for integrable and strongly chaotic situations. Most physical systems are situated in the midst of these limits, however, and belong to what we call 'mixed' systems. The semiclassical theory for mixed systems is difficult and only few aspects have been clarified up to now. This difficulty is associated with the periodic-orbit bifurcations (characteristic to the mixed systems) where the stationary phase approximation (SPA) and the conventional trace formula for representing the quantum spectrum in terms of classical periodic orbits breaks down. Fortunately, however, an approach in the inverse direction sometimes works and one can extract the periodic orbit information from the quantum spectrum by means of the Fourier transformations. This approach is very useful to understand the shell structure of the quantum spectrum. We take this approach and clarify some aspects of a mixed system, directing our attention to the influence of the bifurcations of short periodic orbits on the gross structure of the quantum spectrum.

In this paper, we investigate the classical-quantum correspondence for an axially-symmetric deformed oscillator model with reflection-asymmetric terms. This is a non-integrable model and chaotic behavior gradually emerges in the dynamics as the octupole deformation becomes large. The role of periodic orbit bifurcations will be emphasized. In section 2, basic elements of the semiclassical theory relevant to our analysis are briefly reviewed. Special attention will be paid on the classical bifurcation phenomena and their effects on the quantum spectra. In section 3 our model is introduced and several aspects of it are summarized. In sections 4∼7, we will present numerical results of the semiclassical analysis and discuss their implications. It will be shown that prominent shell structures emerge for finite octupole deformations superposed on the prolate shapes. Origins of such new shell structures will be clarified. Section 8 is devoted to summary and conclusion.

2. BASIC FORMULAE

2.1. Classical Hamiltonian system

Let us consider a Hamiltonian system with f degrees of freedom. The equation of motion (EOM) for a $2f$-dimensional phase space vector $Z = (\boldsymbol{p}, \boldsymbol{q})$ is expressed as

$$\frac{\mathrm{d}}{\mathrm{d}t} Z = \Lambda \frac{\partial H}{\partial Z}, \qquad \Lambda = \begin{pmatrix} O & -I \\ I & O \end{pmatrix}, \tag{2.1}$$

where O and I denote the f-dimensional zero and identical matrices, respectively. Now consider a bundle of trajectories around a certain solution $Z_\alpha(t)$ and write them as $Z(t) = Z_\alpha(t) + \delta Z(t)$. Then the EOM for $\delta Z(t)$ is given by

$$\frac{\mathrm{d}}{\mathrm{d}t} \delta Z = \Lambda \mathcal{H}(Z_\alpha(t))\, \delta Z, \qquad \mathcal{H}(Z)_{ij} = \frac{\partial^2 H(Z)}{\partial Z_i \partial Z_j} \tag{2.2}$$

up to the first order in δZ. $\mathcal{H}$ is called Hessian matrix. One can easily integrate the above differential equation and obtain the following solution:

$$\delta Z(t) = \mathcal{T}_\tau \exp\left[\int_{t_0}^{t} \mathrm{d}\tau \Lambda \mathcal{H}(\tau)\right] \delta Z(t_0) \equiv \mathcal{S}_\alpha(t - t_0)\, \delta Z(t_0), \tag{2.3}$$

where $\mathcal{T}_\tau$ denotes that the exponential is defined by time-ordered product. $\mathcal{S}_\alpha$ is called stability matrix of the trajectory α, whose eigenvalues determine its stability.

Let Σ denote a $(2f-2)$ dimensional hypersurface in the phase space with fixed energy E. It defines a time-discretized mapping $\mathcal{M} : \Sigma \mapsto \Sigma$ with classical trajectories, which is called the Poincaré map. Periodic orbits $\bar{Z}$ are defined as the fixed points of $\mathcal{M}$, namely, by $\mathcal{M}(\bar{Z}) = \bar{Z}$. The linear part M_r (with respect to δZ) of $\mathcal{M}$ about a periodic orbit $\bar{Z}_r$ is called "monodromy matrix" and describes the stability of the orbit:

$$\mathcal{M}(\bar{Z}_r + \delta Z) = \bar{Z}_r + M_r\, \delta Z + \mathcal{O}(\delta Z^2). \tag{2.4}$$

The monodromy matrix is a symplectic matrix satisfying

$$\Lambda\, {M_r}^T\, \Lambda^{-1} = {M_r}^{-1}, \tag{2.5}$$

and this property restricts its eigenvalues as follows. Let λ be one of the eigenvalues of M_r. Relation (2.5) guarantees that the reciprocal of λ is another eigenvalue of M_r. Furthermore, M_r is a real matrix so that the complex conjugates of these eigenvalues are also eigenvalues. Thus the eigenvalues of the monodromy matrix generally appear in quartets ($\mathrm{e}^{\pm\alpha\pm i\beta}$). In the two-dimensional case, they appear in a pair.

Let us now proceed to a discussion on bifurcations of stable periodic orbits. Consider a trajectory that emerges at $\boldsymbol{q}$ with energy E and returns to the initial point, $\boldsymbol{q}' = \boldsymbol{q}$. This kind of trajectory certainly exists for any $\boldsymbol{q}$. The condition for this trajectory to be periodic is that the initial and final momenta coincide; namely, $\boldsymbol{p}' = \boldsymbol{p}$. Using the Hamilton-Jacobi equation, this condition can be rewritten as

$$0 = \boldsymbol{p}' - \boldsymbol{p} = \frac{\partial S(\boldsymbol{q}', \boldsymbol{q}; E)}{\partial \boldsymbol{q}'} - \left(- \frac{\partial S(\boldsymbol{q}', \boldsymbol{q}; E)}{\partial \boldsymbol{q}} \right) = \frac{\partial S(\boldsymbol{q})}{\partial \boldsymbol{q}}, \tag{2.6}$$

where $S(\boldsymbol{q})$ denotes the action integral along the closed path under consideration. Thus, the periodic orbit is the stationary point of this action integral. Let us expand $S(\boldsymbol{q})$ about the periodic point $\bar{\boldsymbol{q}}$:

$$\begin{aligned} S(\bar{\boldsymbol{q}} + \delta\boldsymbol{q}) &= S(\bar{\boldsymbol{q}}) + \frac{1}{2}\, \delta\boldsymbol{q}^T \frac{\partial^2 S(\boldsymbol{q}, \boldsymbol{q})}{\partial \boldsymbol{q} \partial \boldsymbol{q}}\, \delta\boldsymbol{q} + \cdots \\ &\equiv \bar{S} + \frac{1}{2}\, \delta\boldsymbol{q}^T \mathcal{B}\, \delta\boldsymbol{q} + \cdots . \end{aligned} \tag{2.7}$$

After some simple matrix rearrangements, one can express $\mathcal{B}$ in terms of the quadrants of the monodromy matrix as

$$\mathcal{B} = B - (I - A) C^{-1} (I - D), \qquad M \equiv \begin{pmatrix} A & B \\ C & D \end{pmatrix}. \tag{2.8}$$

Note that

$$\det(\mathbf{1} - M) = -\det[C] \det[\mathcal{B}]. \tag{2.9}$$

The above relations provide us with a clear understandings of the connection between eigenvalues of the monodromy matrix and the bifurcation of periodic orbits. Suppose that one of the eigenvalues of M becomes unity. Then the curvature tensor $\mathcal{B}$ for the action S has a zero eigenvalue. This means that the stationary points of S (periodic orbits) locally form a continuous set and a bifurcation can occur hereafter; namely a (few) new stationary point(s) can emerge.

2.2. Trace formula

By means of the semiclassical theory, we can relate properties of the quantum spectrum with those of the corresponding classical system. For non-integrable Hamiltonian systems, the Gutzwiller's trace formula [7–9] represents the quantum level density $g(E) = \sum_i \delta(E - E_i)$ as a sum over classical periodic orbits:

$$g^{(\mathrm{sc})}(E) = \bar{g}(E) + \sum_{r,n} A_{nr}(E) \cos\left(\frac{n S_r(E)}{\hbar} - \frac{\pi}{2} \mu_{nr} \right). \tag{2.10}$$

$\bar{g}(E)$ is called Weyl term (or Thomas-Fermi approximation), which is a monotonic function of energy. The sum is taken over all primitive periodic orbits r and their multiple traversals. $S_r = \oint_r \boldsymbol{p} \cdot d\boldsymbol{q}$ is the action integral along the orbit r, and μ_r denotes the Maslov phase. Several numerical application of this formula to strongly chaotic systems have shown its effectiveness. As is well known, however, exact reproduction of a quantum spectrum is not an easy task, because one has to treat huge number of periodic orbits which show exponential proliferation as a function of energy. On the other hand, since our purpose is to understand the gross structure of the spectrum we need only finite number of periodic orbits which have rather short periods. If one is interested in the gross structure with energy resolution δE, the change of the phase in Eq. (2.10) must be less than 2π for the change of energy by δE. Namely,

$$nS_r(E+\delta E) - nS_r(E) \simeq n\frac{\partial S_r(E)}{\partial E}\delta E = nT_r\delta E \lesssim 2\pi\hbar, \tag{2.11}$$

which leads to the relation

$$nT_r \lesssim T_{\max} \equiv \frac{2\pi\hbar}{\delta E}. \tag{2.12}$$

Thus, we need only short periodic orbits whose periods are less than $T_{\max}$ defined above. Although much efforts have been devoted to reproduce individual eigenenergies by calculating millions of periodic orbits, gross structures of the level spectra have rarely been discussed in connection with periodic orbits for non-integrable systems. (For integrable systems, there are several works; see for instance, Refs. [4,10–13])

2.3. Bifurcations

Let us next discuss the condition for the amplitude factor A_{nr} in the trace formula (2.10) to take a large value. In the stationary phase approximation, the amplitude factor is expressed for isolated orbits as

$$A_{nr} = \frac{1}{\pi\hbar}\frac{T_r}{\sqrt{|\det(\mathbf{1} - {M_r}^n)|}}. \tag{2.13}$$

For degenerate orbits with degeneracy 1, it is represented by

$$A_{nr} = \frac{4\pi}{(2\pi\hbar)^{3/2}}\frac{B_r}{\sqrt{|\det(\mathbf{1} - {M_r}^n)|}}, \qquad B_r = \int_0^{T_r} \mathrm{d}t \left[\frac{\partial\varphi(t+T_r)}{\partial p_\varphi(t)}\right]^{-1/2}, \tag{2.14}$$

where φ and p_φ denote an ignorable variable in the Hamiltonian and its canonically conjugate momentum, respectively (see Appendix in Ref. [14]). From the difference in order of $\hbar$, one sees that the contribution of degenerate orbits is more important than that of isolated ones.

Another important factor, which plays an essential role in our analysis below, is the stability factor $\det(\mathbf{1} - {M_r}^n)$. Its value is independent of the point chosen on the periodic orbit. As discussed above, eigenvalues of the monodromy matrix M_r appear in pairs $(+/-)(\mathrm{e}^{\lambda}, \mathrm{e}^{-\lambda})$, λ being real or pure imaginary, or in quartets $(\mathrm{e}^{\pm\alpha\pm i\beta})$. One should note that the periodic orbit generally appears in at least one parameter family, so that the monodromy matrix

always has two unit eigenvalues. Other pairs of unit eigenvalues correspond to the global continuous symmetries which the Hamiltonian possesses but the orbit itself does not. These degrees of freedom are responsible for the degeneracy and, as seen in Eq. (2.14), can be separated out from the definition of M_r appearing in the stability factor. In the case of three-dimensional systems with axial symmetry, the monodromy matrix has (except for isolated non-degenerate orbits) four unit eigenvalues, and the remaining two appear in a pair $(+/-)(\mathrm{e}^{\lambda}, \mathrm{e}^{-\lambda})$. Thus, M_r may be reduced to a (2×2) matrix for most orbits. λ is purely imaginary for stable orbits, and real for unstable ones. The stability factor for each case becomes

$$\det(\mathbf{1} - M_r) = 2 - \mathrm{Tr}\, M_r$$

with

$$\mathrm{Tr}\, M_r = \begin{cases} 2\cos(\beta) & \text{stable}, \quad \lambda = i\beta \\ \pm 2\cosh(\alpha)) & \text{unstable}, \quad \lambda = \alpha \end{cases} \tag{2.15}$$

Thus, the stability of orbit is determined by the value of $\mathrm{Tr}\, M$.

If a parameter in the Hamiltonian is continuously varied, the periodic orbits change their shapes and the values of λ also change continuously. It may occur that the β for a certain stable orbit becomes a fraction of 2π, namely, $\beta = 2\pi m/n$ with n and m being relatively prime integers. At this point $\mathrm{Tr}\, {M_r}^n$ becomes 2, and the amplitude factor A_{nr} suffers divergence. This singularity corresponds to the period n-upling bifurcation of the orbit r. Near the bifurcation point, the stationary phase approximation breaks down. It is then necessary to take into account higher-order fluctuations about the classical orbit to extract a finite value of A_{nr} [15]. Although we leave this task as an challenging future subject, we expect that the amplitude factor takes large value in the bifurcation region. It will result in a large-amplitude oscillation in the level density, leading to an enhancement of the shell effect.

3. THE MODEL AND ITS SCALING PROPERTIES

3.1. The model

We adopt a model Hamiltonian consisting of an axially deformed harmonic oscillator and a reflection asymmetric octupole deformed potential:

$$H = \frac{p^2}{2M} + \sum_i \frac{M\omega_i^2 x_i^2}{2} - \lambda_{30} M\omega_0^2 \left[r^2 Y_{30}(\Omega)\right]'' . \tag{3.1}$$

Here, the double primes denote that the variables in square brackets are defined in terms of the doubly-stretched coordinates $x_i'' = (\omega_i/\omega_0)x_i$, where $\omega_0 \equiv (\omega_x\omega_y\omega_z)^{1/3}$ being determined so that the volume conservation condition is satisfied [16]. For simplicity, we define dimensionless variables as follows:

$$\begin{cases} p_i & \longrightarrow & \sqrt{M\hbar\omega_0}\, p_i \\ q_i & \longrightarrow & \sqrt{\hbar/M\omega_0}\, q_i \\ H & \longrightarrow & \hbar\omega_0\, H \end{cases} \tag{3.2}$$

Then, the Hamiltonian is written as

$$H = \frac{1}{2}\,p^2 + \frac{1}{2}\,[r^2(1 - 2\lambda_{30}Y_{30}(\Omega))]''. \tag{3.3}$$

Since the radial dependence of the octupole potential is quadratic, the Hamiltonian obeys the following scaling rule:

$$H(\alpha \boldsymbol{p}, \alpha \boldsymbol{q}) = \alpha^2 H(\boldsymbol{p}, \boldsymbol{q}). \tag{3.4}$$

Thanks to this property, if one solves the Hamilton equations of motion at a certain energy E_0, the solution at any energy E is obtained by just scale transforming the solution at E_0 as $Z(t; E) = \sqrt{E/E_0}\, Z(t; E_0)$, Z denoting a phase space vector $(\boldsymbol{p}, \boldsymbol{q})$.

In the cylindrical coordinates (ρ, z, φ), the above Hamiltonian (3.3) is written as

$$H = \frac{1}{2}(p_\rho^2 + p_z^2) + V(\rho, z; p_\varphi),$$

$$V(\rho, z; p_\varphi) = \frac{p_\varphi^2}{2\rho^2} + \left[\frac{\rho^2 + z^2}{2} - \lambda_{30}\sqrt{\frac{7}{16\pi}}\frac{2z^3 - 3z\rho^2}{\sqrt{\rho^2 + z^2}}\right]''. \tag{3.5}$$

Thus, we can treat the system as a two-dimensional one with fixed angular momentum p_φ. This reduction enables us to make use of the Poincaré surface of section in order to survey the classical phase space profile. Note that $\chi \equiv p_\varphi/E$ is a scaling-invariant parameter and, therefore, classical properties are the same for the same χ.

In the following sections, we shall investigate how the properties of the quantum spectrum for the Hamiltonian (3.1) changes as the two deformation parameters, $\delta_{\rm osc} = (\omega_\perp - \omega_z)/\bar{\omega}$ and λ_{30}, are varied. We shall then discuss the physical origins of these changes by means of the periodic orbit theory reviewed in section 2.

3.2. Fourier transformation of quantum level density

As we will see in the following numerical analyses, the Hamiltonian above becomes chaotic with increasing octupole deformation parameter λ_{30}. But considerable parts of the phase space remain regular and the system is considered as a so-called 'mixed system'. The trace formula based on the stationary phase approximation (SPA) does not work well in such situations. The amplitude factors suffer divergences at the bifurcation points of stable periodic orbits because of the breakdown of SPA. Consequently, we cannot directly use the conventional semiclassical expression to analyze the quantum spectrum. Fortunately, we can avoid the above difficulty by using the Fourier transformation technique for the quantum level density. Suppose that the level density is characterized by the classical periodic orbits and is expressed as

$$g_{\rm osc}^{\rm (sc)}(E) = \sum_{n=1}^{\infty}\sum_{r} A_{nr}(E)\,\cos\left(\frac{nS_r(E)}{\hbar} - \frac{\pi}{2}\mu_{nr}\right), \tag{3.6}$$

without specifying the concrete expression of the amplitude factor $A_{nr}(E)$ which may be obtained by going beyond the SPA. Since our model obeys the scaling rule (3.4), energy dependence of the classical variables entering Eq. (3.6) is factored out as follows:

$$\begin{aligned} S_r(E) &= E \cdot T_r, \\ A_{nr}(E) &= E^{d_r/2} A_{nr}^{(0)}, \end{aligned} \tag{3.7}$$

where d_r is the effective degeneracy of the orbit, and equal to 1 for most orbits due to the axial symmetry. For isolated orbits, $d_r = 0$ and we expect that their contributions to the level density may be small. The degeneracies are integers in the classical dynamics, but in the quantum mechanics this restriction is relaxed and d_r changes continuously in the bifurcation regions [15,9]. Using the above relations, Eq. (3.7) is expressed as

$$g^{(\mathrm{sc})}(E) = \bar{g}(E) + \sum_{r,n} E^{d_r/2} A_{nr}^{(0)} \cos\left(\frac{nET_r}{\hbar} - \frac{\pi}{2}\mu_{nr}\right). \tag{3.8}$$

Now let us consider the Fourier transformation of the level density, defined by

$$F(s) = \frac{1}{2\pi\hbar} \int \mathrm{d}E \ \mathrm{e}^{isE/\hbar} \, E^{-d/2} g(E) \cdot \exp\left[-\frac{1}{2}\left(\frac{E}{E_{\max}}\right)^2\right]. \tag{3.9}$$

Here the Gaussian damping factor is used for energy cut-off, and we shall put $d = 1$ in order to cancel the energy dependence of the amplitude factors for most orbits. Inserting the quantum level density $g(E) = \sum_i \delta(E - E_i)$ and the semiclassical one (3.8) into Eq. (3.9), we obtain quantum mechanical and semiclassical expressions for $F(s)$:

$$F^{(\mathrm{qm})}(s) = \frac{1}{2\pi\hbar} \sum_i \frac{1}{\sqrt{E_i}} \, \mathrm{e}^{isE_i/\hbar} \cdot \exp\left[-\frac{1}{2}\left(\frac{E_i}{E_{\max}}\right)^2\right], \tag{3.10}$$

$$F^{(\mathrm{sc})}(s) \simeq \bar{F}(s) + \sum_{r,n} A_{nr}^{(0)} \cdot \frac{1}{\sqrt{2\pi}\Delta s} \exp\left[-\frac{1}{2}\left(\frac{s - nT_r}{\Delta s}\right)^2\right], \tag{3.11}$$

respectively, where $\Delta s = \hbar/E_{\max}$. $F^{(\mathrm{qm})}$ is calculated from the single-particle spectrum obtained by diagonalizing the Hamiltonian with deformed oscillator basis. The result is compared with the semiclassical expression $F^{(\mathrm{sc})}$. In Eq. (3.11), $\bar{F}(s)$ corresponds to the Weyl term which is regarded as a contribution from orbit of zero-length, and it has peak at $s = 0$. The remaining part has a functional form exhibiting successive peaks at the periods of classical periodic orbits and their heights are proportional to the amplitude factors of the corresponding orbits. By comparing the calculated $F^{(\mathrm{qm})}(s)$ with $F^{(\mathrm{sc})}(s)$, we can thus extract information about periodic orbits from the quantum spectrum.

4. SHELL STRUCTURE ENERGY CALCULATION

A useful quantitative measure of shell structure is the shell structure energy which is defined as the fluctuation part of the sum of single-particle energies, i.e.,

$$\mathcal{E}_{\mathrm{sh}}(N) = \sum_{k=1}^{N} E_k - \tilde{\mathcal{E}}(N), \tag{4.1}$$

where E_k's represent eigenvalues of the single-particle Hamiltonian. The second term $\tilde{\mathcal{E}}(N)$ is obtained by smoothing the first term by means of the Strutinsky method; it is a smooth function of particle number N and of other potential parameters. The shell structure energy takes a large negative value when the single-particle level density at the Fermi surface is low.

We have carried out a systematic calculation of the shell structure energy for the Hamiltonian (3.1) as a function of the deformation parameters $\delta_{\rm osc}$ (quadrupole deformation), λ_{30} (octupole deformation) and of the particle number N. Figure 1 shows a map of the local minima of shell structure energies in the two-dimensional deformation parameter space calculated for particle numbers in the range $16 \leq N \leq 160$. The centers of discs show the loci of local minima (corresponding to different values of N) and the sizes of the discs represent the absolute values of shell structure energies. As the order of magnitude of the shell structure energy is roughly proportional to $N^{1/3}$ in the harmonic oscillator case [19], we normalize them by multiplying $N^{-1/3}$ in order to compare system with different values of N.

For $\lambda_{30} = 0$, it is well known that strong shell structure exists at $\delta_{\rm osc} = 0$ (spherical), 3/5 (prolate superdeformed), 6/7 (prolate hyperdeformed), $-3/4$ (oblate superdeformed) and so on. The distribution of discs is actually dense around such points. We find in Fig. 1 that, in addition to such known cases, prominent shell structure emerges also at finite values of octupole deformation. Their shell-structure energies are comparable, in magnitude, to (sometimes larger than) those for the purely quadrupole shapes. The most remarkable region is that of $\lambda_{30} = 0.3 \sim 0.4$ and $\delta_{\rm osc} \simeq 0.1$. Using the semiclassical theory, let us analyze in the following sections the mechanism which creates the above new shell structures for the combination of the quadrupole and octupole deformations.

5. SEMICLASSICAL ANALYSES

In this section, we investigate how the structure of quantum spectrum changes as the octupole deformation parameter λ_{30} is increased, fixing quadrupole deformation parameter $\delta_{\rm osc}$ at several positive values (between the spherical and the prolate superdeformed shapes). Figure 2 shows the single-particle spectra as functions of λ_{30} for the Hamiltonian (3.1) with $\delta_{\rm osc} = 0.1$, 0.3 and 0.5, The corresponding axis ratios $\omega_\perp/\omega_z$ are 31/28, 11/8 and 7/4, respectively. They are not in simple ratios so that there is no prominent shell structure at $\lambda_{30} = 0$. However, new shell structures emerge at finite values of λ_{30}. To see features of these spectra, we show in Fig. 3 the Fourier transforms of the level density defined by (3.10). As discussed in section 3 3.2, one see prominent Fourier peaks at the periods of classical periodic orbits. It means that the fluctuation of the spectrum is characterized by the periodic orbits, demonstrating a beautiful applicability to our model of the semiclassical method in section 2 2.2. For elucidating the features of shell structure, it is essential to understand the behavior of these Fourier peaks with respect to the deformation parameters. As discussed in the previous sections, short periodic orbits play important roles for the formation of gross structure of quantum spectrum. There are various periodic orbits of

various topologies in each part of the deformation parameter space and the same type of orbits change their characters as the parameters change. This fact is clearly seen in the Fourier transforms where peaks corresponding to certain orbits change their heights. The heights of the peaks represent nothing but the strengths of shell structures. Let us discuss in the followings what kind of periodic orbits exist and how they determine the features of quantum spectra in several regions on the $(\delta_{\rm osc}, \lambda_{30})$ plane.

Case of $\delta_{\rm osc} = 0.1$

Let us first take up the case of $\delta_{\rm osc} = 0.1$, where we obtain especially strong shell structures at finite λ_{30} values in the shell structure energy calculation (see Fig. 1), and let us discuss which orbits are responsible for these shell structures. Figure 4 shows, for several values of λ_{30}, some planar periodic orbits in the plane including the symmetry axis. We use the Monodromy Method developed by Baranger et al. [17] to calculate periodic orbits and their monodromy matrices. At $\lambda_{30} = 0$, the most important orbit family is the ellipse-shaped one in the (x, y) plane. The next orbit family is 31:28 Lissageous. They are very long orbits and unimportant for the gross shell structure. Adding the octupole deformation, new types of orbits are born. Orbit PR appears at $\lambda_{30} = 0.12$ by the isochronous bifurcation of the orbit PA, and PA becomes unstable after this bifurcation. At $\lambda_{30} = 0.24$, the orbit PA becomes stable again and a new orbit PM appears.

To see these bifurcations, the Poincaré map is a very convenient implement. As our Hamiltonian has axial symmetry, we can treat it as a two-dimensional system with fixed angular momentum p_φ. Figure 5 is the Poincaré map (z, p_z) for the 'projected' Hamiltonian (3.5) with $p_\varphi = 0$. Here the surface is defined by $p_\rho = 0$ and $\dot{p}_\rho < 0$. In the top panel, the center of the main torus corresponds to the orbit PA. In the middle panel, the orbit PA becomes an unstable saddle and a new pair of island is created. These islands correspond to the orbit PR. In the bottom panel the orbit PA comes back to a stable one and creates a new pair of saddles confronting horizontally. These saddles correspond to the orbit PM.

As is well known, stabilities of periodic orbits are determined by the monodromy matrices. Figure 6 shows the traces of the two-dimensional monodromy matrices for orbits associated with the above bifurcations. The bifurcation occurs at $\mathrm{Tr}\, M = 2$ where the monodromy matrix has the unit eigenvalues $(1, 1)$. Period n-upling bifurcations occur at $\mathrm{Tr}\, M^n = 2$. Higher order (large n) resonances occur at every points of the torus and new orbits bifurcate from them, but they are of rather long periods and are related with more detailed structure of the spectrum. In the Fourier transform Fig. 3(a), the peak corresponding to the orbit PA with period $T \simeq 2\pi/\omega_\perp$ strongly enhances at $\lambda_{30} \simeq 0.2$. It mainly characterizes the shell structure seen in the spectrum Fig. 2(a) at $\lambda_{30} = 0.2 \sim 0.3$. This enhancement is related with the above bifurcations of PA at $\lambda_{30} = 0.128$ and 0.227.

Case of $\delta_{\rm osc} = 0.3$

Next let us discuss the case of $\delta_{\rm osc} = 0.3$. Some important classical orbits are drawn in Fig. 7. Orbit PO is born out of the period-doubling bifurcation of the orbit IL at $\lambda_{30} = 0.215$. Orbits PP and PQ are created by the saddle-node bifurcation (pair creation of stable and unstable orbits from nothing) at $\lambda_{30} = 0.221$. Orbit PR emerges from the isochronous bifurcation of the orbit PA at $\lambda_{30} = 0.338$. In the Fourier transform Fig. 3(b), the enhancement of the peak with $s \simeq 1$ is related with the isochronous bifurcation. The orbits associated with the period-doubling and saddle-node bifurcations mentioned above are of similar periods and contribute to the same peak with $s \simeq 2.75$ in the Fourier transform. It also shows strong enhancement in the bifurcation region.

Case of $\delta_{\rm osc} = 0.5$

Lastly, let us consider the case of $\delta_{\rm osc} = 0.5$. This quadrupole deformation is almost equivalent to the case of axis ratio $\sqrt{3} : 1$ treated in Ref. [18]. The feature of shell is rather weak at $\lambda_{30} = 0$. However, one may notice in Fig. 2 that a remarkable shell structure emerges at $\lambda_{30} \simeq 0.3$. In the Fourier transform Fig. 3(c), a significant enhancement of the peak with $s \simeq 1.75$ is observed. It seems that this is the most typical example in our model, which clearly exhibits a new shell structure emerging at finite octupole deformation.

Some short periodic orbits are illustrated in Fig. 8. At $\lambda_{30} = 0$, the ellipse-shaped family in the (x, y) plane characterize the structure of the spectrum. Orbit PB is born out of the isochronous bifurcation of the orbit IL at $\lambda_{30} = 0.276$, orbits PC and PD are created by the saddle-node bifurcation at $\lambda_{30} = 0.274$. The Poincaré maps and the traces of the monodromy matrices are displayed in Figs. 9 and 10, respectively. The strong enhancement of the peak with $s \simeq 1.85$ at $\lambda_{30} \simeq 0.4$ are related with the bifurcations mentioned above. Orbits associated with these bifurcations are of similar periods and thus contribute to the same peak in the Fourier transform Fig 3(c). These bifurcations may be regarded as the mechanism which creates the prominent shell structure at finite octupole deformation.

Orbits PE and PF are born associated with the period-tripling bifurcation of the orbit PA at $\lambda_{30} = 0.376$. A quantum signature of this bifurcation is also seen in the Fourier peak with $s \simeq 3$. Thus, we can conclude that the enhancement of Fourier peak in the bifurcation region is a general phenomenon.

6. BIFURCATION LINES IN THE TWO-DIMENSIONAL PARAMETER SPACE

In the preceding section, we presented several examples where bifurcations of short periodic orbits play important roles in forming shell structures. In this section, let us discuss roles of the bifurcations varying two deformation parameters systematically. In the n-dimensional parameter space, bifurcation points generally form $(n-1)$-dimensional manifolds; they are 1-dimensional curves in the present case. We have evaluated these bifurca-

tion lines for some short periodic orbits. The result of calculation is presented in Figure 11. These bifurcation lines always emerge at the points where the ratios $\omega_\perp/\omega_z$ are rational and $\lambda_{30} = 0$. Note that $\delta_{\rm osc}$=0, 3/5, 6/7 and $-3/4$ correspond to the spherical, prolate superdeformed, prolate hyperdeformed and oblate superdeformed shapes, respectively. The orbit PA causes isochronous bifurcations along the lines `i` and `ii` (in direction from the right to the left). As discussed in the case $\delta_{\rm osc} = 0.1$, new orbits PM and PR are born after the bifurcations `i` and `ii`, respectively. On the other hand, as discussed in the case $\delta_{\rm osc} = 0.5$, the lines `iii`$\sim$`vi` are related with the orbits PB, PC, PD, IL and 2PA (double traversals of the orbit PA). The orbit IL causes isochronous bifurcation (from the left to the right) and produces the orbit PB along the line `iii`, while the orbit PC (unstable) and PD (stable) are born out of the saddle-node bifurcation along the line `iv` in the region $\delta_{\rm osc} \lesssim 0.5$. As $\delta_{\rm osc}$ increases, orbits PB and PC exchange their stabilities with each other along the line `v` and annihilate into 2PA along the line `vi`. Along the line `vii`, the orbit PA causes period-tripling bifurcation (from the right to the left) and produces orbits PE and PF.

According to the discussions in the preceding sections, we expect strong shell effects along these bifurcation lines. Prominent shell structures are known to exist for the spherical and superdeformed shapes (the end points of the bifurcation lines) where periodic orbit conditions for the harmonic oscillator potential are satisfied. Conditions for the emergence of pronounced shell structure in non-integrable systems are not well known, however. As is indicated in Fig. 1, shell structure energies at equilibrium shapes with finite λ_{30} are comparable in magnitude to those of spherical and superdeformed shapes. The most remarkable one is the region with $\delta_{\rm osc} \simeq 0.1$ and $\lambda_{30} = 0.3 \sim 0.4$. The bifurcation map of Fig. 11 suggests that the strong shell effect in this region may be connected with the bifurcation of orbit PA (the lines `i` and `ii`). In fact, we saw in the preceding section that the Fourier peak corresponding to the orbit PA is strongly enhanced by the bifurcation phenomena. It is worth emphasizing that such a strong shell effect can arise associated with classical orbit bifurcations in non-integrable systems.

One should also note that most of the large discs in Fig. 1 at finite λ_{30} locate in the prolate side ($\delta_{\rm osc} > 0$). This is related with the property of the shortest periodic orbit: For prolate shapes, the shortest orbit is of the type-PA. It is degenerate and stable, so its contribution to the level density is important. On the other hand, the shortest orbit for oblate shapes is of the type-IL, which is isolated and, accordingly, its contribution to the level density is rather small. The orbit of type-PA, the second shortest orbit, is unstable against the octupole deformation, and less important in comparison with the prolate case. A more detailed discussion on the difference in stability between the oblate and prolate superdeformed shapes against octupole deformations will be given in the next section. The same problem was discussed also in [20,21] from somewhat different point of view.

7. OCTUPOLE DEFORMATION SUPERPOSED ON THE PROLATE AND OBLATE SUPERDEFORMATIONS

Let us discuss the origin of the difference in octupole stability between the prolate and oblate superdeformed states. In Ref. [16,14] we have shown that the supershell effect in the prolate superdeformed states increases with increasing octupole deformation. As an underlying mechanism of that enhancement, we emphasized the importance of stability properties of two kinds of periodic orbit family and of their interference effect. The oblate case is similar to the prolate case in that there are two kinds of periodic orbit family whose periods are in the ratio 2:1. But the structure of quantum spectrum is quite different with each other. In Fig. 12 are compared the single-particle spectra for the prolate ($\omega_\perp/\omega_z = 2$) and oblate ($\omega_\perp/\omega_z = 1/2$) superdeformed oscillators as functions of the octupole deformation parameter λ_{30}. The way the degeneracy be solved is different between the two. The octupole operator Y_{30} has matrix elements between states in the same major shell in the oblate case and, therefore, it affects the spectrum in the first order perturbation, while it affects only in the second order in the prolate case. Let us discuss below how this difference be explained in terms of the classical dynamics point of view. For this purpose, representative periodic orbits with short periods are displayed in Fig. 14 for several octupole deformation parameters λ_{30}.

We first compare the features of the two spectra without the octupole term. Figure 13 shows the oscillating level density smoothed to an energy width $\delta E = \omega_{\rm sh}/2$ ($\omega_{\rm sh}$ being the energy spacing between adjacent major shells). A characteristic feature is that the prolate superdeformed spectrum has an undulating pattern (supershell structure) while oblate one does not. This is due to the difference in degeneracies of contributing periodic orbits. As discussed in Ref. [14], two orbit families (corresponding to orbits (PB, PC) and orbit PA in the upper panel of Fig. 14, respectively) in the prolate superdeformed states have degeneracies 4 and 2. In the oblate case, the orbit family with period $2\pi/\omega_\perp$ (corresponding to orbits (PA, PL) in the lower panel of Fig. 14 has the maximal degeneracy 4, but the shortest orbit (the linear orbit IL along the z-axis) is isolated and has degeneracy 1. Thus the interference effect between these two families is so small that one cannot see the supershell effect in the spectrum.

Figure 15 compare the Fourier transforms of the level density for the prolate and oblate cases. One can hardly see the component at $s = 1$ in the oblate case and the oscillating pattern of the spectrum is determined by the $s = 2$ component almost exclusively. Comparing the two figures, one notice that the reduction rate of the peak-height due to the octupole deformation is much greater in the oblate case. This rapid decline clearly corresponds to the rapid disappearance of the shell effect in the oblate case.

The main reason for reduction of the shell effect with increasing octupole deformation is two-fold: The first is the reduction of degeneracy of the periodic orbit families, and the second is the change of stabilities. As the degeneracies are the same for the major orbit families in both cases (orbits PB, PC, $\cdots$ in the prolate case and orbits PA, PL, $\cdots$ in the oblate case), we expect that the differences are associated mainly with the stability

properties. In Fig. 16 we show the stability factors $X \equiv \sqrt{|\det(1-M_r)|}$ calculated as function of λ_{30}. The stability factors for orbits in the oblate potential depend linearly on λ_{30} for $\lambda_{30} \simeq 0$ while they depend quadratically in the prolate case. Consequently the amplitude factors reduce much faster in the former case. This seem to be the main cause of the rapid reduction of shells with octupole deformation in the oblate potential.

8. SUMMARY AND CONCLUSION

We have analyzed the gross structure of single-particle spectra in reflection-asymmetric deformed oscillator potentials using the semiclassical method. Our model is non-integrable and is regarded as a mixed system where regular and chaotic dynamics coexist. The periodic orbit theory, which is well established for regular and strongly chaotic limits, seems to be also applicable to such a situation. Fourier transforms of the quantum level density reveal almost perfect correspondences with classical periodic orbits. Importance of classical orbit bifurcations has been demonstrated in our model. Strong shell effects arise also for rather chaotic regions, and their strengths are comparable in magnitude to those of regular regions. We obtain an interesting result which indicates that classical bifurcations may be responsible for the emergence of shell structure in the mixed system. Applications of the semiclassical theory of shell structure to more realistic mean-field potential models and identifications of classical orbits which play decisive roles in determining exotic shapes of nuclei or micro-clusters remain as exciting future subjects.

ACKNOWLEDGEMENTS

The authors thank Dr. M. Matsuo (Yukawa Institute for Theoretical Physics) and Dr. H. Aiba (Koka Women's College) for fruitful discussions.

---

[1] S. Åberg, H. Flocard and W. Nazarewicz, Ann. Rev. Nucl. Part. Sci. 40 (1990) 439.

[2] W. Nazarewicz, P. Olanders, I. Ragnarsson, J. Dudek, G. A. Leander, P. Möller and E. Ruchowska, Nucl. Phys. A429 (1984) 269.

[3] S. Mizutori, T. Nakatsukasa, K. Arita, Y. R. Shimizu and K. Matsuyanagi, Nucl. Phys. A557 (1993) 125c.

[4] H. Nishioka, Klavs Hansen and B. R. Mottelson, Phys. Rev. B42 (1990), 9377.

[5] S. Frauendorf and V. V. Pashkevich, Rossendorf preprint FZR-37 (1993).

[6] D. Heiss and R. G. Nazmitdinov, preprint (1994), to appear in Phys. Rev. Lett.

[7] M. C. Gutzwiller, J. Math. Phys. 8 (1967) 1979; 12 (1971) 343.

[8] M. C. Gutzwiller, Chaos in Quantum and Classical Mechanics, (Springer Verlag, 1990).

[9] A. M. Ozorio de Almeida, Hamiltonian System: Chaos and Quantization, (Cambridge University Press, 1988).

[10] R. Balian and C. Bloch, Ann. of Phys. 69 (1972) 76.

[11] M. V. Berry and M. Tabor, Proc. Roy. Soc. Lond. A349 (1976) 101.

[12] A. G. Magner, V. M. Kolomietz and V. M. Strutinsky, Sov. J. Nucl. Phys. 28 (1978) 764.

[13] H. Frisk, Nucl. Phys. A511 (1990) 309.

[14] K. Arita, Prog. Theor. Phys. 90 (1993) 747.
K. Arita and K. Matsuyanagi, Prog. Theor. Phys. 91 (1994) 723.

[15] A. M. Ozorio de Almeida and J. H. Hannay, J. of Phys. A20 (1987) 5873.

[16] K. Arita and K. Matsuyanagi, Prog. Theor. Phys. 89 (1993), 389.

[17] M. Baranger, K. T. R. Davies and J. H. Mahoney, Ann. of Phys. 186 (1988) 95.

[18] K. Arita, Phys. Lett. B336 (1994) 279.

[19] A. Bohr and B. R. Mottelson, Nuclear Structure, vol.2 (Benjamin, New York, 1975), p. 585.

[20] W. D. Heiss, R. G. Nazmitdinov and S. Radu, Phys. Rev. Lett. 72 (1994) 2351.

[21] W. D. Heiss, R. G. Nazmitdinov and S. Radu, Phys. Rev. B51 (1995-I) 1874.

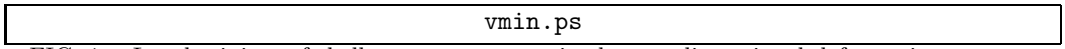

FIG. 1. Local minima of shell structure energy in the two-dimensional deformation parameter space $(\delta_{\rm osc}, \lambda_{30})$. Size of each disc represents the absolute value of the shell structure energy normalized as $\mathcal{E}_{\rm sh}/N^{1/3}$. Plotted are for even N in the range $16 \le N \le 160$.

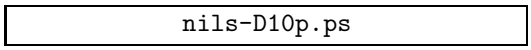

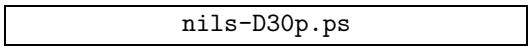

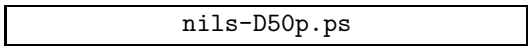

FIG. 2. Single-particle spectrum of the Hamiltonian (3.1) with deformation parameter $\delta_{\rm osc} = 0.1$, 0.3 and 0.5 as functions of the octupole parameter λ_{30}. Dashed and solid curves represent the levels whose K quantum numbers are zero and nonzero, and the latter degenerate in two due to the time-reversal symmetry.

(a) $\delta_{\rm osc} = 0.1$

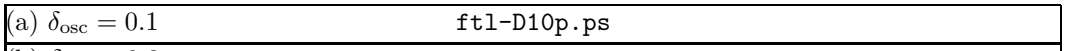

(b) $\delta_{\rm osc} = 0.3$

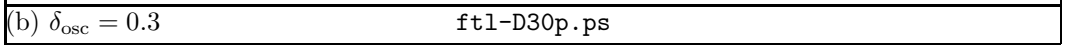

Fig. 3, to continue.

(c) $\delta_{\rm osc} = 0.5$

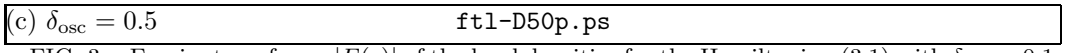

FIG. 3. Fourier transforms $|F(s)|$ of the level densities for the Hamiltonian (3.1) with $\delta_{\rm osc} = 0.1$, 0.3 and 0.5, plotted as functions of the action s and the octupole parameter λ_{30}.

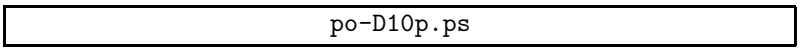

FIG. 4. Some short planar periodic orbits of the Hamiltonian (3.1) with $\delta_{\rm osc} = 0.1$.

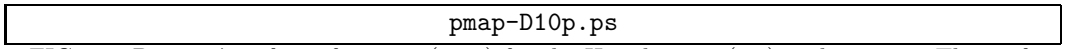

FIG. 5. Poincaré surface of section (z, p_z) for the Hamiltonian (3.5) with $p_\varphi = 0$. The surface is defined by $p_\rho = 0$ and $\dot{p}_\rho < 0$.

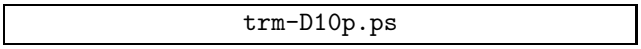

FIG. 6. Traces of the Monodromy matrices at $\delta_{\rm osc} = 0.1$ for some short periodic orbits plotted as functions of the octupole deformation parameter λ_{30}.

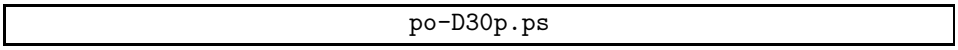

FIG. 7. Some short planar periodic orbits for the Hamiltonian (3.1) with $\delta_{\rm osc} = 0.3$.

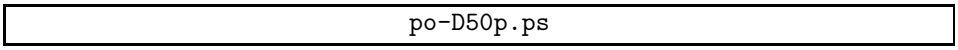

FIG. 8. Some short planar periodic orbits for the Hamiltonian (3.1) with $\delta_{\rm osc} = 0.5$.

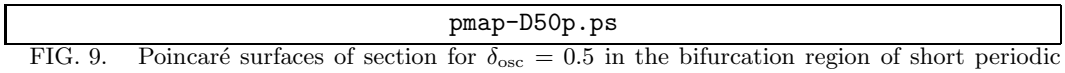

FIG. 9. Poincaré surfaces of section for $\delta_{\rm osc} = 0.5$ in the bifurcation region of short periodic orbits. The surface (ρ, p_ρ) is defined by $z = 0$ and $p_z > 0$.

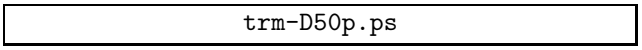

FIG. 10. Same as Fig. 6 but $\delta_{\rm osc} = 0.5$.

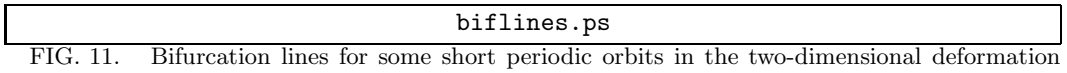

FIG. 11. Bifurcation lines for some short periodic orbits in the two-dimensional deformation parameter space $(\delta_{\rm osc}, \lambda_{30})$.

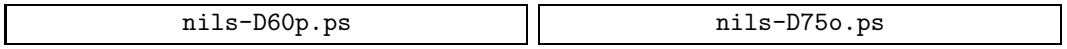

FIG. 12. Single-particle spectra for (a) prolate and (b) oblate superdeformed oscillators plotted as functions of the octupole deformation parameter λ_{30}.

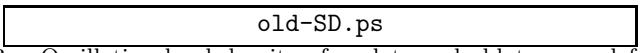

FIG. 13. Oscillating level density of prolate and oblate superdeformed oscillators, which are smoothed to an energy width $\delta E = \hbar\omega_{\rm sh}/2$.

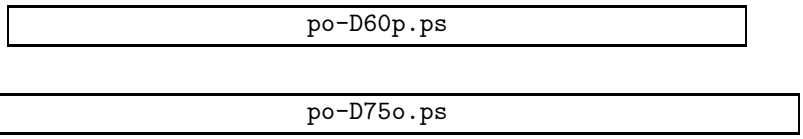

FIG. 14. Some short periodic orbits in the prolate (upper panel) and the oblate (lower panel) superdeformed potentials with octupole deformations.

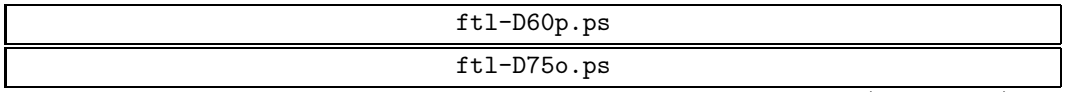

FIG. 15. Fourier transforms of the quantum level densities for the prolate (upper panel) and the oblate (lower panel) superdeformed oscillators with octupole deformations.

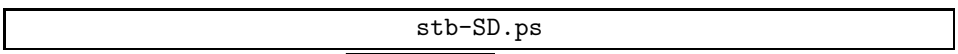

FIG. 16. Stability factors $X = \sqrt{|\det(1 - M_r)|}$ of the short periodic orbits for the prolate (left) and the oblate (right) superdeformed potentials plotted as functions of the octupole deformation parameter λ_{30}. The sign of X is that of $\det(M_r - 1) = {\rm Tr}\, M_r - 2$. Namely, $-2 < X \leq 0$ for stable orbits and otherwise for unstable ones.